Skewness of Gabor Wavelets and Source Signal Separation

Weichuan Yu
Dept. of Diagnostic Radiology
Yale University
weichuan@noodle.med.yale.edu

Gerald Sommer
Institut für Informatik
University Kiel
gs@ks.informatik.uni-kiel.de

Kostas Daniilidis
GRASP Laboratory
University of Pennsylvania
kostas@grasp.cis.upenn.edu

Abstract

Responses of Gabor wavelets in the mid-frequency space build a local spectral representation scheme with optimal properties regarding the time-frequency uncertainty principle. However, when using Gabor wavelets we observe a skewness in the mid-frequency space caused by the spreading effect of Gabor wavelets. Though in most current applications the skewness does not obstruct the sampling of the spectral domain, it affects the identification and separation of source signals from the filter response in the mid-frequency space. In this paper, we present a modification of the original Gabor filter, the skew Gabor filter, which corrects skewness so that the filter response can be described with a sum-of-Gaussians model in the mid-frequency space. The correction further enables us to use higher-order moment information to separate different source signal components. This provides us with an elegant framework to deblur the filter response which is not characterized by the limited spectral resolution of other local spectral representations.

1 Introduction

Gabor filters [13] are very attractive due to their optimal localization properties both in spatial and in spectral domain. According to the well known uncertainty principle, the product of the spatial and the spectral support of a filter has a lower bound. Because Gaussians and modulated Gaussians (Gabor functions) can achieve such a lower bound they are very useful in many spectral analysis tasks such as image representation (e.g. [20]) and the spatio-temporal analysis of motions in image sequences (e.g. [1, 15]). Besides, Gabor filters were shown to approximate biological models of vision (e.g. [7, 19, 16]). In the spatio-temporal models for motion estimation [1, 2], the energy spectrum of a constant translational motion can be characterized as an oriented plane passing through the origin in the spectral domain. Sampling the spectrum with a set of Gabor filters at different frequencies and orientations [15] may help us to estimate the orientation of the spectral plane. Grzywacz and Yuille [14] further argued that the spectral support of a Gabor filter is a measure of uncertainty and the angle between two tangential lines of the support, which pass through the spectral origin, represents the uncertainty of orientation estimation (see figure 1). This angle is desired to be the same for filters at different frequencies. Thus, the spectral support should be proportional to the distance between the origin and the support center.

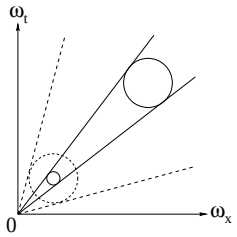

Figure 1: The motivation of applying 2D Gabor wavelets (redrawn from [14]). We represent the spectral support of a 2D Gabor filter with a circle. Applying a set of filters with constant scale may cause larger angular uncertainty at lower frequencies (as shown by the angle between two dashed lines). Thus, the spectral support of filters should be directly proportional to the mid-frequency.

In Gabor filters, impulse responses have the same support in low and hig frequencies. However, we would prefer the support to be inversely proportional to the mid-frequency. The coupling of the bandwidth with the mid-frequency yields Gabor wavelets, a combination of Gabor filter and wavelets [21, 6], extensively used in signal analysis and image representation (e.g. [20, 27]).

In applying Gabor wavelets we observe a positive skewness in the mid-frequency space [14]. This skewness did not draw considerable attention in the computer vision community because most applications of Gabor wavelets are classification tasks. Being aware of the non-symmetrically spreading effect of Gabor wavelets in the mid-frequency space, we argue that an isotropic dissemination of the mid-frequency representation of the filter response (we call this local spectral representation the *mid-spectrum*) may facilitate the deblurring of filter responses so that we no more suffer from the limited resolution of frequency-based approaches. This is especially useful in source signal separation and multiple spectral orientation analysis. Based on this motivation we design a new filter to correct this skewness effect (section 2). In section 3 we further describe the 1D corrected mid-spectrum with a sum-of-Gaussians model and use higher-order moments to identify different source components. The deblurring of the mid-spectrum is also demonstrated. In section 4 we extend the analysis to 2D spectral orientation analysis. This paper is concluded with some discussions in section 5.

2 The Skewness of Gabor Wavelets

We first explain the positive skewness of Gabor wavelets. For simplicity we begin with a 1D Gabor filter whose impulse response reads

$$g_1(x;\omega_0,\sigma_x) := \frac{1}{\sqrt{2\pi}\sigma_x} e^{-(\frac{x^2}{2\sigma_x^2})} e^{j\omega_0 x}. \tag{1}$$

Here ω_0 denotes the mid-frequency and σ_x is the scale parameter. The spectrum of $g_1(x;\omega_0,\sigma_x)$ is a Gaussian centered at ω_0

$$G_1(\omega;\omega_0,\sigma_x) = e^{-\frac{\sigma_x^2(\omega-\omega_0)^2}{2}} \tag{2}$$

with bandwidth inversely proportional to σ_x. In applications, we usually calculate the spatial convolution between $g_1(x;\omega_0,\sigma_x)$ and the input signal $i(x)$

$$h_1(x;\omega_0,\sigma_x) := i(x) * g_1(x) = \int_{\xi=-\infty}^{\infty} i(\xi) g_1(x-\xi) d\xi. \tag{3}$$

At a fixed position x_0, the filter response is simplified as an inner product

$$h_1(x_0;\omega_0,\sigma_x) = \int_{\xi=-\infty}^{\infty} i(\xi) g_1(x_0-\xi) d\xi. \tag{4}$$

Using the facts that $g_1(x_0-x) = g_1^\star(x-x_0)$ and $G_1^\star(\omega) = G_1(\omega)$ (here $\star$ denotes conjugation) the above inner product can also be represented in the spectral domain according to the Parseval theorem ([4], pp.113-115) as

$$h_1(x_0;\omega_0,\sigma_x) = \int_{\omega=-\infty}^{\infty} I(\omega) G_1(\omega) e^{j\omega x_0} d\omega. \tag{5}$$

Here $I(\omega)$ is the spectrum of $i(x)$. Thus, for $x = x_0$ (for simplicity we set $x_0 = 0$) we obtain a local spectral representation which is a function of the mid-frequency ω_0 and the scale σ_x. We call this representation the mid-spectrum of the signal.

The mid-spectrum $h_1(\omega_0, \sigma_x)$ spreads every spectral Dirac component of the source signal into a function of ω_0. Assume that the spectrum of a source signal is a Dirac function: $I(\omega) = \delta(\omega - \omega_i)$ originating from a complex harmonic. Equation (5) then turns out to be

$$h_1(\omega_0, \sigma_x) = G_1(\omega_i; \omega_0, \sigma_x) = e^{-\frac{\sigma_x^2(\omega_0 - \omega_i)^2}{2}}. \tag{6}$$

When the parameter σ_x is a constant, $h_1(\omega_0, \sigma_x)$ is a Gaussian spreading of $\delta(\omega - \omega_i)$ and there is no skewness. But if the wavelet property is preferred, i.e. if σ_x is inversely proportional to ω_0

$$\sigma_x = \frac{C}{\omega_0} \tag{7}$$

with C as a constant. Then, we observe the positive skewness of ω_0 [14] (see also figure 2)

$$h_1(\omega_0, C) = e^{-\frac{C^2(\omega_0 - \omega_i)^2}{2\omega_0^2}}. \tag{8}$$

We may straightforwardly extend the above analysis for n-dimensional Gabor wavelets with isotropic envelope. For 2D Gabor wavelets in the spatio-temporal domain we have the following relation

$$\sigma_x = \sigma_t = \frac{C}{\sqrt{\omega_{x0}^2 + \omega_{t0}^2}}. \tag{9}$$

The mid-spectrum of a 2D spectral impulse $\delta(\omega_{x0} - \omega_{xi}, \omega_{t0} - \omega_{ti})$ reads

$$h_2(\omega_{x0}, \omega_{t0}, C) = \exp\{-\frac{C^2(\omega_{x0} - \omega_{xi})^2 + (\omega_{t0} - \omega_{ti})^2}{2(\omega_{x0}^2 + \omega_{t0}^2)}\}. \tag{10}$$

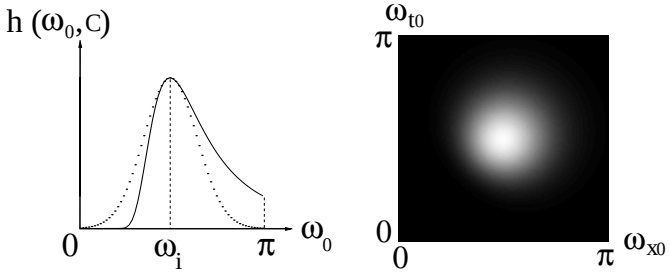

Figure 2: The skewness of Gabor wavelets. **Left:** The solid curve denotes $h_1(\omega_0, C)$ and the dotted curve is a Gaussian function centered at ω_i with the scale parameter $\frac{\omega_i}{C}$. $C = 3.5, \omega_i = \frac{\pi}{2}$. **Right:** 2D skewness $h_2(\omega_{x0}, \omega_{t0}, C)$. $C = 3.5, \omega_{xi} = \omega_{ti} = \frac{\pi}{2}$.

In many Gabor wavelet approaches, this skewness seems harmless because it does not obstruct the description of different signals with a set of samples [18, 22]. The main attention was attracted to the efficient covering/sampling of the spectrum as well as the coefficient estimation of the Gabor basis [3, 20]. But we should keep in mind that the spreading effect of Gabor wavelet filtering (see equation (8)) really blurs the input signal non-symmetrically in the mid-frequency space. For the sake of source signal identification and separation, we prefer to have a symmetric spreading. In the following we present a new filter to correct this positive skewness.

2.1 Correcting the Skewness

In order to achieve symmetry in the mid-spectrum, we introduce a new skew Gabor filter whose spectral definition reads

$$SG_1(\omega; \omega_0, C) := \exp\{-(\frac{C^2}{2})(\frac{\omega - \omega_0}{\omega})^2\}. \tag{11}$$

There exists no analytical expression of the skew Gabor filter in the spatial domain because there is no closed-form representation of the inverse Fourier transform of $SG_1(\omega)$. But we may obtain an FIR version of both the real and the imaginary part of the skew Gabor filter $sg_1(x)$ using filter-design in the Fourier domain and discrete Fourier transform. In figure 3 we display one example of the skew Gabor filter. It is similar to a Gabor filter with subtle shape differences inside the Gaussian envelope.

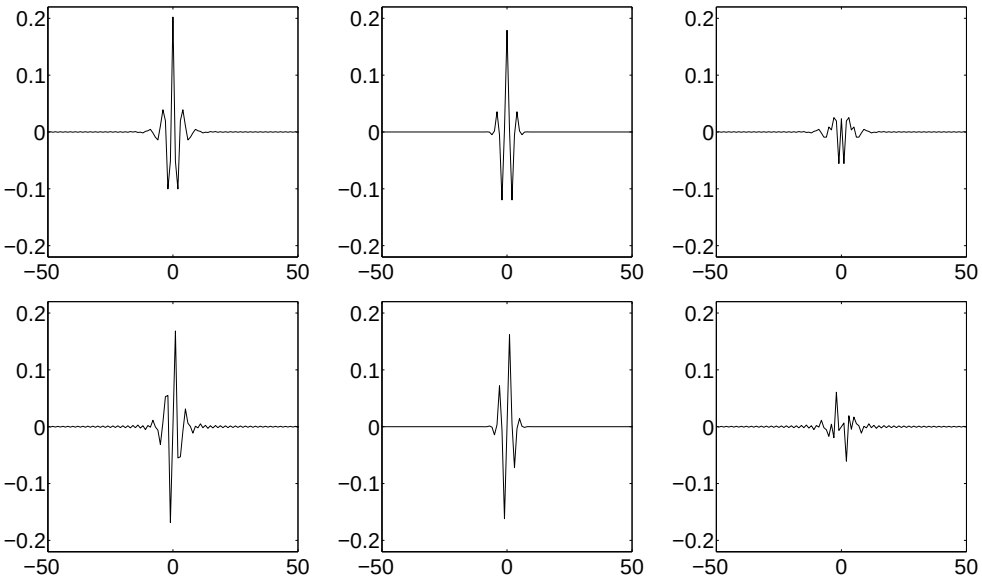

Figure 3: **Top:** The real parts of a 1D skew Gabor filter (left) and of a Gabor filter (middle) as well as their even-symmetric difference (right). **Bottom:** The imaginary parts of both filters (left: skew Gabor; middle: Gabor) and their odd-symmetric difference (right). The parameters are $C = 3.5$ and $\omega_0 = \frac{\pi}{2}$.

Replacing $G_1(\omega; \omega_0, \sigma_x)$ in equation (5) with $SG_1(\omega; \omega_0, \sigma_x)$ yields a mid-spectrum with an ideal Gaussian shape

$$sh_1(\omega_0, C) = \exp\{-\frac{C^2(\omega_0 - \omega_i)^2}{2\omega_i^2}\}. \tag{12}$$

Similarly, we may correct the skewness of 2D Gabor wavelets by using a 2D skew Gabor filter

$$SG_2(\omega_x, \omega_t; \omega_{x0}, \omega_{t0}, C) = \exp\{-(\frac{C^2}{2})[\frac{(\omega_x - \omega_{x0})^2 + (\omega_t - \omega_{t0})^2}{\omega_x^2 + \omega_t^2}]\}. \tag{13}$$

The mid-spectrum corresponding to $\delta(\omega_{x0} - \omega_{xi}, \omega_{t0} - \omega_{ti})$ is then an ideal 2D Gaussian (cf. equation (10))

$$sh_2(\omega_{x0}, \omega_{t0}, C) = \exp\{-(\frac{C^2}{2})[\frac{(\omega_{x0} - \omega_{xi})^2 + (\omega_{t0} - \omega_{ti})^2}{\omega_{xi}^2 + \omega_{ti}^2}]\}. \tag{14}$$

In figure 4 we display a 1D cosine sequence and the correction of the skewness in the mid-spectrum. Here we use only one constant C to keep the Gaussian envelope isotropic. It is also possible to apply two different constants (i.e. $C_x \neq C_t$) in order to form a mid-spectrum with an elongated Gaussian shape . But this is beyond the scope of this paper.

3 1D Source Signal Separation

In the following we demonstrate the merit of correcting the positive skewness. We start with 1D source signal separation. We assume that the spectrum of an input signal is composed of two Dirac components

$$S(\omega) = a_1\delta(\omega - \mu_1) + a_2\delta(\omega - \mu_2), \tag{15}$$

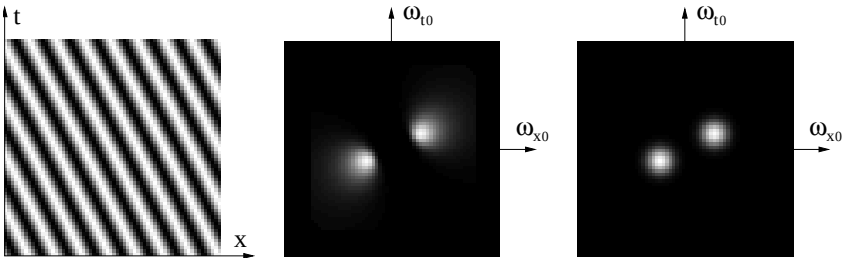

Figure 4: **Left:** Cosine sequence $f(x,t) = 5\ \cos(\frac{\pi}{4}(x+0.5t))$. **Middle:** Mid-spectrum using Gabor wavelets with $C = 3.5$. **Right:** Mid-spectrum using 2D skew Gabor filters with the same C. The skewness in the middle image is corrected.

where their amplitudes (a_1 and a_2) and offsets (μ_1 and μ_2) are unknown. Our goal is to estimate these amplitudes and offsets from the mid-spectrum so that the source components can be identified and separated. Here we do not discuss the traditional Fourier analysis, but focus on the comparison with Gabor wavelets.

If we apply plain Gabor wavelets for filtering, the mid-spectrum is an overlap of two skewness curves (cf. equation (8)). Though iterative algorithms (e.g. [8, 23]) or learning methods (e.g. [9]) may be used to extract the desired parameters, such non-analytic approaches are computationally inefficient and are sensitive to initial values and related parameters in the cost function. Besides, they are susceptible to local minima in the regression procedure. Thus, we prefer to use an analytic framework for parameter regression.

The correction of skewness makes this idea possible. Under the same assumption as that in equation (15), the mid-spectrum of skew Gabor filters is then a sum of two differently weighted and shifted Gaussian functions (for simplicity we omit the coefficient term $\frac{1}{\sqrt{2\pi}\sigma}$ of Gaussian)

$$g(\omega_0) = g_1(\omega_0) + g_2(\omega_0) \tag{16}$$

with

$$\begin{cases} g_1(\omega_0) &= a_1 e^{-\frac{(\omega_0-\mu_1)^2}{2(\frac{\mu_1}{C})^2}} \\ g_2(\omega_0) &= a_2 e^{-\frac{(\omega_0-\mu_2)^2}{2(\frac{\mu_2}{C})^2}} \end{cases} . \tag{17}$$

The scale parameters in above Gaussians are proportional to the mean values. In figure 5 we demonstrate the mid-spectrum of plain Gabor wavelet filtering as well as the mid-spectrum of skew Gabor filtering.

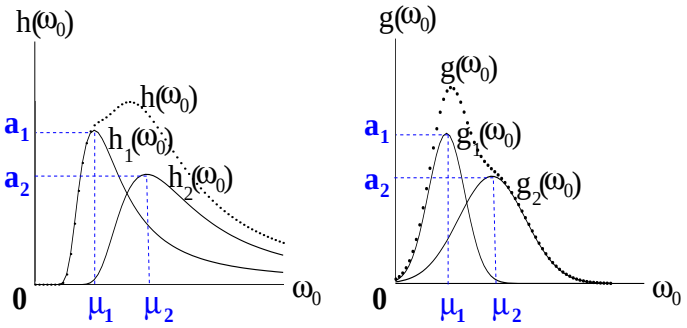

Figure 5: **Left:** The mid-spectrum of plain Gabor wavelet filtering. **Right:** The superposition of two Gaussians after 1D skew Gabor filtering. We have totally four unknowns: the amplitudes a_1 and a_2 as well as the mean values μ_1 and μ_2. The scale parameters of these two Gaussians are determined by $\frac{\mu_1}{C}$ and $\frac{\mu_2}{C}$, respectively.

The sum-of-Gaussians model is well studied from statistic aspect and is widely used in neural network approaches (e.g. [9, 23]). One more benefit of this model is that we are able to use higher-order moment information to extract

parameters. According to Appendix A we obtain the following system of equations in a_1, a_2, μ_1, and μ_2

$$\begin{cases} a_1\mu_1 + a_2\mu_2 &=& m_0\frac{C}{\sqrt{2\pi}} &:=& b_1 \\ a_1\mu_1^2 + a_2\mu_2^2 &=& m_1 b_1 &:=& b_2 \\ a_1\mu_1^3 + a_2\mu_2^3 &=& \frac{1}{\frac{1}{C^2}+1} m_2 b_1 &:=& b_3 \\ a_1\mu_1^4 + a_2\mu_2^4 &=& \frac{1}{\frac{3}{C^2}+1} m_3 b_1 &:=& b_4 \end{cases} . \tag{18}$$

Here m_0 denotes the integration of $g(\omega_0)$ and m_1, m_2, and m_3 denote the first three order moments of $g(\omega_0)/m_0$. Without loss of generality we assume $0 < \mu_1 \leq \mu_2$. Solving these equations (Appendix B) yields

$$\begin{cases} a_1 &=& \frac{a(2ab_2+bb_1+b_1\sqrt{b^2-4ac})}{b^2-4ac-b\sqrt{b^2-4ac}} \\ a_2 &=& \frac{a(2ab_2+bb_1-b_1\sqrt{b^2-4ac})}{b^2-4ac+b\sqrt{b^2-4ac}} \\ \mu_1 &=& \frac{-b+\sqrt{b^2-4ac}}{2a} \\ \mu_2 &=& \frac{-b-\sqrt{b^2-4ac}}{2a} \end{cases} , \tag{19}$$

where b_1, b_2, b_3, and b_4 are defined in (18) and the variables a, b, and c are defined in (B.6) (Appendix B). The term $b^2 - 4ac$ is guaranteed to be no less than zero (see Appendix B). If $b^2 - 4ac = 0$, there is only one single Gaussian (i.e. $\mu_1 = \mu_2$) and we can estimate its mean value and amplitude directly using equations (A.1) and (A.2).

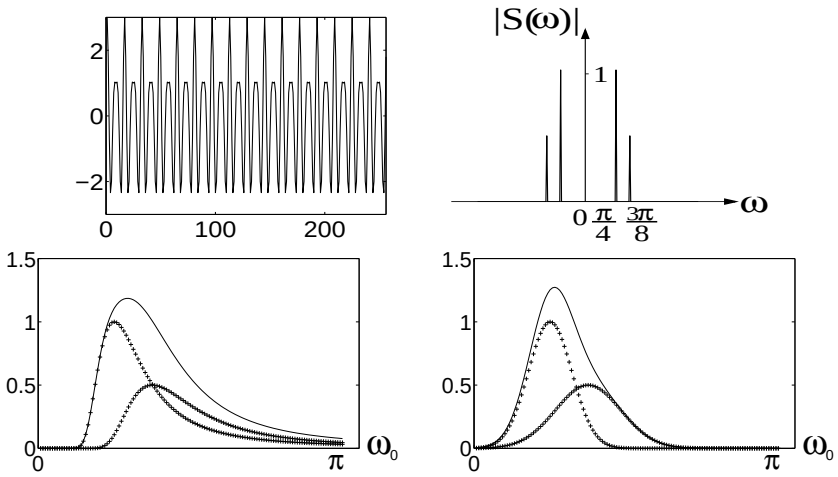

Figure 6: **Top:** The source signal and its energy spectrum. **Bottom:** The positive mid-spectra (solid lines) using plain Gabor wavelets (left) and using skew Gabor filters (right). These curves are actually overlapping of the spreading responses of two Dirac functions (shown as crosses).

In figure 6 we display an example of source signal separation. The input signal is composed of two cosine functions

$$s(x) = 2\cos(\frac{\pi}{4}x) + \cos(\frac{3\pi}{8}x) \tag{20}$$

with the spectrum $S(\omega) = \delta(\omega \pm \frac{\pi}{4}) + \frac{1}{2}\delta(\omega \pm \frac{3\pi}{8})$. Now we sample the positive spectral space with Gabor wavelets and skew Gabor filters. We start the mid-frequency at $\omega_0 = \frac{\pi}{128}$ and increase it with a step of $\frac{\pi}{128}$ to get a dense sampling. Here we set the highest mid-frequency as $\omega_0 = \frac{7\pi}{8}$ so that we do not need to consider the boundaries in the mid-spectrum. Using higher-order moments we estimate the amplitudes and the locations of two positive Dirac components

$$\begin{cases} a_1 &=& 0.9976 &\approx 1 \\ a_2 &=& 0.4825 &\approx \frac{1}{2} \\ \mu_1 &=& 0.8130 &\approx \frac{\pi}{4} \\ \mu_2 &=& 1.2079 &\approx \frac{3\pi}{8} \end{cases} . \tag{21}$$

In the negative frequencies, we may perform a similar procedure to extract the desired parameters. Then, we are able to identify the source signal components in spite of the blurring in the mid-spectrum. In other words, this method can "deblur" the mid-spectrum. Taking into account that a lot of efforts had to be made in filter design so that the blurring after filtering does not significantly affect the identification of signals or orientations (e.g. [25, 28]), this framework provides an elegant solution which increases the resolution in mid-frequency space.

4 Orientation Analysis in 2D Spectral Space

In this section, we analyze the appearance of multiple orientations in 2D spectral space using skew Gabor filters. An important application of this analysis is multiple motion analysis in xt-space. According to [11, 12, 2], both 1D occlusion and transparency may be modeled as multiple lines in the spectral domain, with some distortion in case of occlusion and without distortion in case of transparency. Thus, the problem of motion estimation turns out to be an issue of orientation analysis in the spatio-temporal space. As the angle between two spectral lines can be arbitrary, eigen-analysis (e.g. [24, 17]) cannot properly determine the orientation of multiple lines. Sampling the spectrum with Gabor filters [15] provided a good motivation, but suffered under the limited resolution. Here we prove that this limitation may be overcome using skew Gabor filters.

As the energy spectrum of either occlusion or transparency is mainly a superposition of two spectral lines, the corresponding mid-spectrum after skew Gabor filtering is then the sum of differently weighted 2D Gaussians centered on two spectral lines. Along each spectral line, these Gaussians have the same angular uncertainty due to wavelet property (cf. figure 1). Though the angular distribution $sh_a(\theta)$ of a 2D Gaussian is no more an exact 1D Gaussian, we still can approximate $sh_a(\theta)$ using a Gaussian with appropriate parameters, especially if C is adequately large (e.g. $C \geq 3$). Due to the space limitation we won't delve into the mathematic derivation, but use an example in figure 7 as an intuitive proof. The reader is referred to [29] for more details. After this approximation, all 2D Gaussians centered on the same spectral line have the same angular mean value and the same angular scale parameter σ_a. Consequently, after polar integration [1] we obtain one 1D Gaussian from all 2D Gaussians centered on the same spectral line and the angular distribution of the mid-spectrum is the superposition of two 1D Gaussians. Thus, we are able to extract the exact orientation of the spectral lines from the blurring mid-spectrum using the framework introduced in section 3. The only difference here is that the parameter σ_a is no more proportional to θ_i, but a constant determined by C.

4.1 Examples

To evaluate the performance of our framework properly, we use synthesized examples. The first example demonstrates the deblurring ability of our framework. We use a 2D signal whose spectrum is composed of two spectral lines passing through the origin (figure 8). The angles between these two lines and the ω_x axis are 15 degrees and 30 degrees, respectively. The mid-spectrum after skew Gabor filtering is strongly blurred due to the spreading effect of filtering and the overlapping of two neighboring Gaussians. The source signal components are hardly to observe in this mid-spectrum. Using higher-order moments, we are still able to determine the orientation of the original spectral lines: $\mu_1 = 13.37°$ and $\mu_2 = 30.07°$. The relative large error in μ_1 is caused by the discrete approximation of the polar integration (e.g. at 0 degree we have more grid points than at 15 degrees). We may reduce this error by increasing the grid density or by interpolation. But we will not enter this topic here.

[1] This integration is well known as Radon Transform [26].

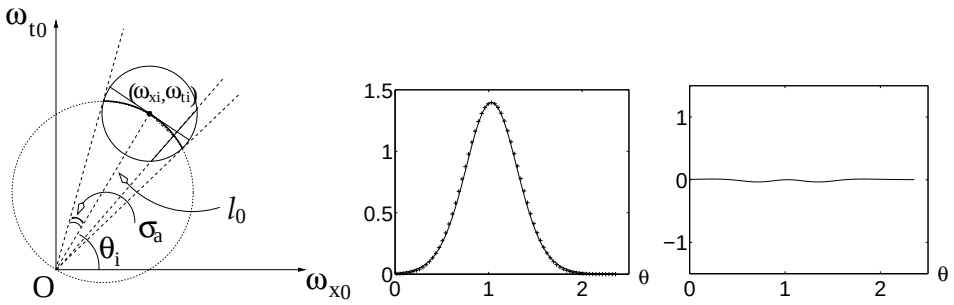

Figure 7: **Left:** Polar integration of an isotropic 2D Gaussian centered at $(\omega_{xi}, \omega_{ti})$ can be approximated by an ideal Gaussian function with mean value θ_i and scale parameter σ_a. The solid circle represents the support of the Gaussian. The pencil of lines passing through the origin denotes the integration paths. The middle point of the intersection between a integration path and the solid circle lies on the dotted circle with a diameter l_0. **Middle:** The solid curve is the plot of $sh_a(\theta)$. For comparison we plot an ideal Gaussian with crosses as well. The scale of this Gaussian is $\sigma_a = \sin^{-1}(1/C)$ with $C = 3.5$. **Right:** The maximal difference between the normal Gaussian and $sh_a(\theta)$ is less than 2% of $\max(sh_a(\theta_i))$.

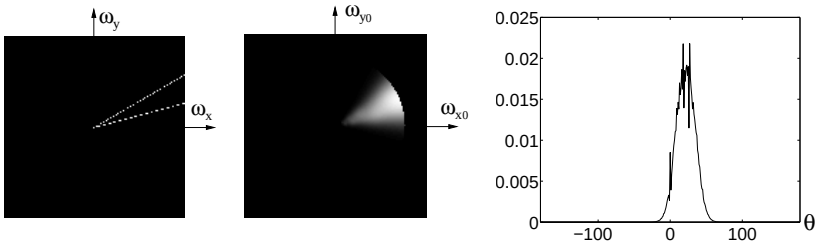

Figure 8: **Left:** The spectrum of a 2D signal is composed of two spectral lines passing through the origin with an angle of 15 degrees between them. **Middle:** Mid-spectrum using 2D skew Gabor filters with $C = 6$. The mid-frequency satisfies $\pi/16 \leq \sqrt{\omega_{x0}^2 + \omega_{t0}^2} \leq 3\pi/4$. **Right:** The angular distribution of the mid-spectrum.

The second example is to estimate multiple motions in a transparency sequence (figure 9). In this sequence we have one random dot sequence moving at 1.00 [pixel/frame] and one sum-of-cosines sequence moving at 0.40 [pixel/frame], respectively. For clarity of displaying we arrange the maximal amplitude of the cosine sequence to be twice the maximal amplitude of the random dot sequence so that the corresponding spectral lines have the same amplitudes. The spectrum displays the superposition of two motions clearly. The mid-spectrum spreads this distribution. This is clearly to see in the plot after the polar integration. As the spectral lines are symmetric with respect to the origin, we only need one half for estimation. Here we use the higher-order moments in the angular space between 90 degrees and 180 degrees to determine the orientation of spectral lines: $\mu_1 = 134.43^\circ$ and $\mu_2 = 158.62^\circ$. The normal vector of these two lines indicate the velocities: $u_1 = \cot(\mu_1 - 90^\circ) = 1.02$ and $u_2 = \cot(\mu_2 - 90^\circ) = 0.39$.

5 Discussions

The skewness correction of Gabor wavelets results in a Gaussian spreading of the input signal in the mid-frequency space. After the correction we are able to model the distribution in the parameter space with a sum of Gaussian functions. Comparing with the non-symmetric skewness curve, the benefit of using Gaussian functions for distribution description is obvious: Gaussians have good localization ability and are capable of providing simple yet rich descriptions of signals. From the point of view of probabilistic signal processing and pattern recognition, this

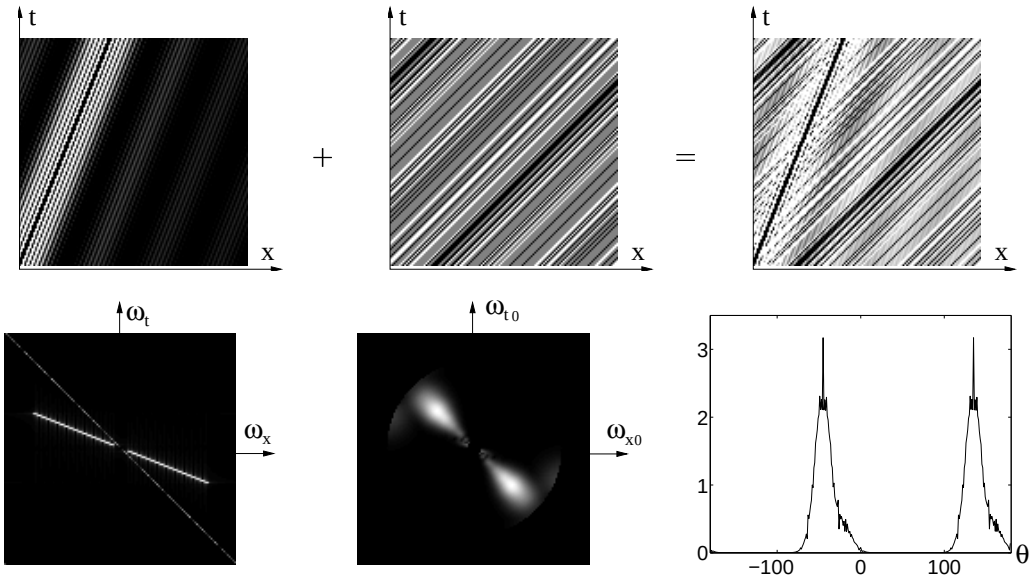

Figure 9: **Top:** The transparency sequence (right) $f(x,t) = \sum_{k=1}^{89} A_k \cos(\omega_k(x-0.4t)+\phi_k)+ran(x-t)$. In the sum-of-cosine sequence (left) ω_k varies from $\pi/16$ to $3\pi/4$ with a step of $\pi/128$. The amplitudes A_k and phase components ϕ_k are randomly chosen. The random dot sequence (middle) $ran(x-t)$ moves with 1 [pixel/frame]. **Bottom Left:** The spectrum of the transparency sequence. **Bottom Middle :** Mid-spectrum using 2D skew Gabor filters with $C = 6$. The middle frequency satisfies $\pi/16 \leq \sqrt{\omega_{x0}^2 + \omega_{t0}^2} \leq 3\pi/4$. **Bottom Right:** The angular distribution of the mid-spectrum.

correction simplifies the tasks of signal analysis significantly. For example, the analytical framework for source signal separation benefits from the statistical simplicity of Gaussians in calculating higher-order moments.

Higher-order moment information is also used in independent component analysis (ICA) approaches [5, 10]. In ICA approaches we need a numerical solution (e.g. singular value decomposition (SVD)) because the distribution is unknown. In our framework, however, the sum-of-Gaussian model makes an analytic solution possible. It is also worth mentioning that we need only one superposition of the source signals to separate them (In [10], for example, two linearly independent superposition are needed to separate source signals).

Another point of our source signal separation framework is that most frequency-based methods suffer from low resolution due to spreading and overlapping. By achieving the spreading to have a Gaussian shape, we can separate two overlapping Gaussians in the mid-frequency space. This enables us to reach very fine resolution in the spectral domain and therefore solve the aliasing problem.

In the future work the following points are worth studying:

- Extend the framework to 2D multiple motion analysis, where the source signal itself is a sum of 2D Gaussians.
- Reduce the computational load by using elongated filter masks and by studying how sparsely we can sample the spectrum without affecting the parameter regression.
- Develop efficient estimation algorithms for the spectrum with multiple harmonics (more than two Dirac impulses).
- Study the sensitivity to noise.

Appendix A

For convenience we change the variable in equations (16) and (17) to x and normalize $g_1(x)$, $g_2(x)$, and $g(x)$ to obtain the corresponding distribution density functions $f_1(x)$, $f_2(x)$, and $f(x)$:

$$m_0 = \int g(x)dx = \frac{\sqrt{2\pi}}{C}(a_1\mu_1 + a_2\mu_2), \tag{A.1}$$

$$\begin{cases} f_1(x) = \frac{g_1(x)}{\int g_1(x)dx} = \frac{1}{\frac{\sqrt{2\pi}}{C}\mu_1} e^{-\frac{(x-\mu_1)^2}{2(\frac{\mu_1}{C})^2}} \\ f_2(x) = \frac{g_2(x)}{\int g_2(x)dx} = \frac{1}{\frac{\sqrt{2\pi}}{C}\mu_2} e^{-\frac{(x-\mu_2)^2}{2(\frac{\mu_2}{C})^2}} \\ f(x) = \frac{1}{m_0}g(x) = \frac{1}{a_1\mu_1+a_2\mu_2}[a_1\mu_1 f_1(x) + a_2\mu_2 f_2(x)] \end{cases}.$$

The first three order moments of $f(x)$ read

$$m_1 = \int xf(x)dx = \frac{1}{a_1\mu_1 + a_2\mu_2}(a_1\mu_1^2 + a_2\mu_2^2), \tag{A.2}$$

$$m_2 = \int x^2 f(x)dx = \frac{\frac{1}{C^2}+1}{a_1\mu_1 + a_2\mu_2}(a_1\mu_1^3 + a_2\mu_2^3), \tag{A.3}$$

$$m_3 = \int x^3 f(x)dx = \frac{\frac{3}{C^2}+1}{a_1\mu_1 + a_2\mu_2}(a_1\mu_1^4 + a_2\mu_2^4). \tag{A.4}$$

Reformulate equations (A.1), (A.2), (A.3), and (A.4) yields the equation system (18).

Appendix B

After defining $x_1 = a_1\mu_1$, $x_2 = a_2\mu_2$, we get an equation system of variables x_1, x_2, μ_1, and μ_2 from (18)

$$x_1 + x_2 = b_1, \tag{B.1}$$

$$x_1\mu_1 + x_2\mu_2 = b_2, \tag{B.2}$$

$$x_1\mu_1^2 + x_2\mu_2^2 = b_3, \tag{B.3}$$

$$x_1\mu_1^3 + x_2\mu_2^3 = b_4. \tag{B.4}$$

From (B.1) and (B.2) we obtain

$$x_1(\mu_1 - \mu_2) = b_2 - b_1\mu_2, \tag{B.1-1}$$

$$x_2(\mu_1 - \mu_2) = b_1\mu_1 - b_2. \tag{B.2-1}$$

We multiply both sides of (B.3) and (B.4) with $(\mu_1 - \mu_2)$ and simplify them as

$$(b_2 - b_1\mu_1)\mu_2 = b_3 - b_2\mu_1, \tag{B.3-1}$$

$$(b_2 - b_1\mu_1)\mu_2^2 + (b_2 - b_1\mu_1)\mu_1\mu_2 + b_2\mu_1^2 - b_4 = 0. \tag{B.4-1}$$

Submitting (B.3-1) into (B.4-1) yields

$$a\mu_1^2 + b\mu_1 + c = 0 \tag{B.5}$$

with

$$\left\{ \begin{array}{lcl} a & := & b_2^2 - b_1 b_3 \\ b & := & b_1 b_4 - b_2 b_3 \\ c & := & b_3^2 - b_2 b_4 \end{array} \right. . \tag{B.6}$$

This is a standard one variable, two order equation whose discriminator reads

$$\begin{array}{rcl} b^2 - 4ac & = & (b_1 b_4 - b_2 b_3)^2 - 4(b_2^2 - b_1 b_3)(b_3^2 - b_2 b_4) \\ & = & [a_1 a_2 \mu_1 \mu_2 (\mu_1 - \mu_2)^3]^2 \geq 0 \end{array} \tag{B.7}$$

The equality is attainable only when $\mu_1 = \mu_2$, i.e. when we have only one single Gaussian. Then we only need to use (A.1) and (A.2) directly to extract parameters. In case of $b^2 - 4ac > 0$, we have two real roots (without loss of generality we assume $\mu_1 < \mu_2$)

$$\left\{ \begin{array}{lcl} \mu_1 & = & \frac{-b+\sqrt{b^2-4ac}}{2a} \\ \mu_2 & = & \frac{-b-\sqrt{b^2-4ac}}{2a} \end{array} \right. . \tag{B.8}$$

Submitting μ_1 and μ_2 into (B.1-1) and (B.2-1) and further taking into account that $x_1 = a_1\mu_1$, $x_2 = a_2\mu_2$ we solve a_1 and a_2

$$\left\{ \begin{array}{lcl} a_1 & = & \frac{a(2ab_2 + bb_1 + b_1\sqrt{b^2-4ac})}{b^2-4ac-b\sqrt{b^2-4ac}} \\ a_2 & = & \frac{a(2ab_2 + bb_1 - b_1\sqrt{b^2-4ac})}{b^2-4ac+b\sqrt{b^2-4ac}} \end{array} \right. . \tag{B.9}$$

References

[1] E. H. Adelson and J. R. Bergen. Spatiotemporal energy models for the perception of motion. *Journal of the Optical Society of America*, 1(2):284–299, 1985.

[2] S.S. Beauchemin and J.L. Barron. The frequency structure of 1d occluding image signals. *IEEE Trans. Pattern Analysis and Machine Intelligence*, 22:200–206, 2000.

[3] A. C. Bovik, M. Clark, and W. S. Geisler. Multichannel texture analysis using localized spatial filters. *IEEE Trans. Pattern Analysis and Machine Intelligence*, 12(1):55–73, 1990.

[4] R. N. Bracewell. *The Fourier Transform and Its Applications*. McGraw-Hill Book Company, 1986.

[5] J. Cardoso. Source separation using higher order moments. In *IEEE International Conf. on Acoustics, Speech and Signal Processing*, pages 2109–2112, 1989.

[6] K. Daubechies. *Ten Lectures on Wavelets*. Society for Industrial and Applied Mathematics, 1992.

[7] J. G. Daugman. Uncertainty relation for resolution in space, spatial frequency and orientation optimized by two-dimensional visual cortical filters. *Journal of the Optical Society of America*, 2(7):1160–1169, 1985.

[8] J. G. Daugman. An information-theoretic view of analog representation in striate cortex. In E. L. SChwartz, editor, *Computational Neuroscience*, pages 403–423. MIT Press, 1990.

[9] J.G. Daugman. Complete discrete 2-d Gabor transforms by neural networks for image analysis and compression. *IEEE Transactions on ASSP*, 36(7), 1988.

[10] H. Farid and E. H. Adelson. Separating reflections from images using independent components analysis. *Journal of the Optical Society of America*, 16(9):2136–2145, 1999.

[11] D. J. Fleet. *Measurement of Image Velocity*. Kluwer Academic Publishers, 1992.

[12] D.J. Fleet and K. Langley. Computational analysis of non-Fourier motion. *Vision Research*, 34:3057–3079, 1994.

[13] D. Gabor. Theory of communication. *Journal of the IEE*, 93:429–457, 1946.

[14] N.M. Grzywacz and A.L. Yuille. A model for the estimate of local image velocity by cells in the visual cortex. *Proc. Royal Society of London.*, B 239:129–161, 1990.

[15] D. J. Heeger. Optical flow using spatiotemporal filters. *International Journal of Computer Vision*, 1(4):279–302, 1987.

[16] F. Heitger, L. Rosenthaler, R. Von der Heydt, E. Peterhans, and O. Kuebler. Simulation of neural contour mechanisms: from simple to end-stopped cells. *Vision Research*, 32(5):963–981, 1992.

[17] B. Jähne. *Spatio-Temporal Image Processing*. Springer-Verlag, 1993.

[18] A.K. Jain and F. Farrokhnia. Unsupervised texture segmentation using Gabor filters. *Pattern Recognition*, 24(12):1167–1186, 1991.

[19] J.J. Koenderink and A.J. Van Doorn. Representation of local geometry in the vision system. *Biological Cybernetics*, 55:367–375, 1987.

[20] T. S. Lee. Image representation using 2D Gabor wavelets. *IEEE Trans. Pattern Analysis and Machine Intelligence*, 18(10):959–971, 1996.

[21] S. G. Mallat. A theory for multiresolution signal decomposition: The wavelet representation. *IEEE Trans. Pattern Analysis and Machine Intelligence*, 11(7):674–693, 1989.

[22] B.S. Manjunath and W.Y. Ma. Texture features for browsing and retrieval of image data. *IEEE Trans. Pattern Analysis and Machine Intelligence*, 18(8):837–842, 1996.

[23] T. Poggio and F. Girosi. Networks for approximatation and learning. *Proceedings of the IEEE*, 78(9):1481–1497, 1990.

[24] M. Shizawa and K. Mase. A unified computational theory for motion transparency and motion boundaries based on eigenenergy analysis. In *IEEE Conf. Computer Vision and Pattern Recognition*, pages 289–295, Maui, Hawaii, June 3-6, 1991.

[25] E. P. Simoncelli and H. Farid. Steerable wedge filters for local orientation analysis. *IEEE Trans. Image Processing*, 5(9):1377–1382, 1996.

[26] J. Radon, translated by P. C. Parks. On the determination of functions from their integral values along certain manifolds. *IEEETMI*, 5(4):170–176, 1986.

[27] R. P. Würtz. Object recognition robust under translations, deformations, and changes in background. *IEEE Trans. Pattern Analysis and Machine Intelligence*, 19(7):769–774, 1997.

[28] W. Yu, K. Daniilidis, and G. Sommer. Approximate orientation steerability based on angular Gaussians. *IEEE Trans. Image Processing*, 10(2):193–205, 2001.

[29] W. Yu, G. Sommer, and K. Daniilidis. Skewness of Gabor wavelets and source signal separation. *submitted to IEEE Trans. Signal Processing*, 2001.